Radiative and Collision-Induced Relaxation of Atomic States in the $2p^5 3p$ Configuration of Neon†*

W. R. BENNETT, JR.‡ AND P. J. KINDLMANN§
Sloane and Dunham Laboratories, Yale University, New Haven, Connecticut
(Received 21 February 1966)

Application of techniques previously developed by the authors for the precise measurement of excited-state lifetimes has been made to radiative and collision-induced relaxation in the ten fine-structure levels of the $2p^5 3p$ configuration of atomic neon. Lifetimes are determined as a function of pressure by studying the transient decay of isolated optical transitions from levels excited by short bursts of threshold-energy electrons. Measurements of the total radiative lifetimes have been made for these ten states within errors ranging from about 1 to 3%. The present work represents an improvement in the accuracy with which these lifetimes have been determined of at least an order of magnitude over previous experimental determinations. Discrepancies (which in some cases amount to an order of magnitude in the mean values) with previous lifetime studies are shown to be easily attributable to radiative cascade effects arising from non-threshold excitation. The radiative lifetimes for these levels (Paschen notation) are, in nsec: $2p_1(14.4\pm0.3)$; $2p_2(18.8\pm0.3)$; $2p_3(17.6\pm0.2)$; $2p_4(19.1\pm0.3)$; $2p_5(19.9\pm0.4)$; $2p_6(19.7\pm0.2)$; $2p_7(19.9\pm0.4)$; $2p_8(19.8\pm0.2)$; $2p_9(19.4\pm0.6)$; and $2p_{10}(24.8\pm0.4)$. Variations $\approx 5\%$ in the radial part of the transition probability were encountered for different $3p \rightarrow 3s$ transitions; these variations may be attributed to configuration interaction. Calculations of σ^2 from the Coulomb approximation agreed with the experimentally determined values within this spread. Cross sections for inelastic excitation transfer were encountered for the more closely spaced states which were comparable to gas kinetic cross sections, but which could not be determined in the present work to within much less than 50% error in most cases. The relationship of the present work to problems in the gas laser field is discussed.

I. INTRODUCTION

WE have been concerned with the development of general and precise methods for the study of relaxation processes in short-lived excited states in gases. Our interest in this problem ranges from specific applications to laser physics and astrophysics to a more general desire to investigate the nature of inelastic excited state collision processes and the accuracy of calculated oscillator strengths. In previous papers we have reviewed the various sources of interpretational difficulty and systematic error inherent with such measurements[1,2] and have discussed the present experimental method in some detail.[2,3] Consequently, in the present paper we shall merely summarize the relevant interpretational considerations and the experimental technique we have devised. The main emphasis in the present paper will be placed on our final results for the $2p^5 3p$ configuration of neon.[2]

II. EXPERIMENTAL METHOD

The excited state lifetimes are determined directly from the transient decay of isolated optical transitions after the sharp removal of a pulsed source of excitation. The method is shown schematically in Fig. 1. Excitation is accomplished with short bursts of threshold energy electrons which are applied periodically at a rate of 100 kc/sec. Because of the low excited-state densities and over-all detection efficiency, the probability of one decaying atom being detected per gun pulse is small compared to unity. Consequently, a pulse-counting method is used to determine the average probability of the atom decaying as a function of time through repeated application of the excitation pulse. The method is thus analogous to the delayed coincidence experiment of Heron, McWhirter and Rhoderick,[4] with the exception that the greatly increased sensitivity of a multichannel delayed coincidence analyzer is incorporated in the experiment. This increased sensitivity has had the enormous practical advantage of permitting data to be taken at threshold energy,

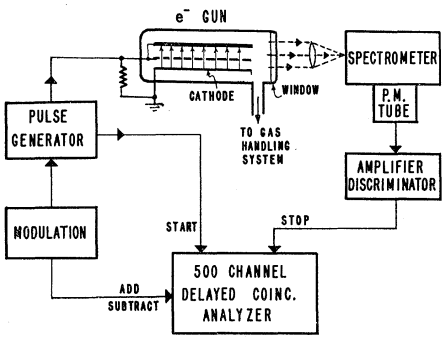

FIG. 1. Schematic diagram of the apparatus.

† This research has been supported in part by the Air Force Office of Scientific Research.

* A preliminary report of this study of the $2p^5\,3p$ configuration was given in Ref. 2.

‡ Alfred P. Sloan Foundation Fellow.

§ To be submitted in partial fulfillment of the requirements for the Doctor of Philosophy degree at Yale University.

[1] W. R. Bennett, Jr., in *Advances in Quantum Electronics*, edited by J. Singer (Columbia University Press, New York, 1961), pp. 28–43.

[2] W. R. Bennett, Jr., P. J. Kindlmann, and G. N. Mercer, Appl. Opt. Suppl. 2, 34 (1965).

[3] P. J. Kindlmann and J.Sunderl and, Rev. Sci. Instr. 37, 445 (1966).

[4] S. Heron, R. W. P. McWhirter and E. H. Rhoderick, Nature 174, 564 (1954); Proc. Roy. Soc. (London) A234, 565 (1956).

thereby eliminating a source of order of magnitude error from radiative cascade processes. The use of multichannel, delayed-coincidence techniques in this type of measurement was first made by one of us through application of an analogue time calibration method in the study of this same configuration of neon.[1,5] Sources of differential channel nonlinearity inherent to that approach were found to result in a significant fraction of the limiting error, however, and digital methods of time analysis were therefore investigated.

The digital method of time analysis finally adopted in this work utilizes a phase-locked vernier chronotron developed by Kindlmann and Sunderland.[3] The basic principles of this time sorting method are illustrated in Fig. 2. Two pulse recirculation loops are used which differ in time delay by approximately 2 nsec out of 1-μsec. The recirculation amplifiers in both loops are gated in phase with a crystal-controlled 500 Mc/sec oscillator, thereby insuring that the time delays in these two loops are made to differ by an amount which is locked precisely to 2 nsec. A 'start' pulse is applied to the input of the longer circulation loop, which is derived from the excitation pulse applied to the electron gun, and delayed by an amount equal to the duration of the excitation pulse and transit time in the photoelectron detection circuitry. If no photoelectron pulse is detected which corresponds to the first 1-μsec interval after application of the gun pulse, the 'start' pulse merely circulates once and the circuit is reset. However, if an excited state decay is detected which corresponds to the first 1-μsec time interval after removal of the gun pulse, it causes a pulse to start circulating in the shorter loop shown at the right in Fig. 2. A 1-Mc/sec scaler across the output of the second loop counts the number of recirculations N required for the delayed pulse to catch up with the pulse circulating in the first loop. The latter event is determined by the output of the coincidence circuit in Fig. 2, and it is apparent that the time interval T between the 'start' pulse and the delayed photoelectron pulse is then given by

$$T = 2N \text{ nsec}.$$

The accuracy of the time-interval measurement is limited only by the stability of the reference oscillator and the transit time variation in the phase-locked recirculation amplifiers. The output of the time interval measuring circuit is fed to a standard 500-channel magnetic core memory having a capacity of 1 million counts per channel. The differential nonlinearity of the over-all system has been found experimentally to be $\leqq 0.1\%$, the limiting statistical uncertainty imposed by the counting capacity of the analyzer. Systematic errors arising from the saturable nature of the vernier chronotron are entirely negligible for the low counting rates in the experiment. The final errors in measured excited state lifetimes which we obtain in practice are limited entirely by statistical considerations and by departures from a pure exponential form in the excited-state decay. The time resolution (≈ 4 nsec) of the over-all experiment is limited primarily by the drift velocity of electrons in the gun and was determined from the low-pressure decay of the He(3^1P) term.

The electron gun is used in a diode arrangement and the applied voltage pulse is shaped to have a monotonically increasing wave form of about 100 nsec duration until it reaches a level ≈ 0.1 to 0.2 eV above the threshold energy for the state. This excitation pulse is turned off with a decay time $\leqq 2$ nsec. The electron current flux is typically ≈ 5 mA/cm^2 during the excitation pulse and the duty-cycle is sufficiently low to prevent a significant effect from any multiple step excitation processes. The upper end of the electron energy distribution cuts off within 0.1 to 0.2 eV of the applied voltage pulse, as determined by the sharpness of the excitation function of representative levels near threshold, and appears limited by the cathode temperature. The lower end of the electron energy distribution presumably varies spatially because of space charge effects over a range of a few volts. Additional assurance that the transient decay of atoms excited by threshold energy electrons is actually what is being studied is obtained through use of a slow, periodic modulation of the pulse amplitude about the threshold energy and an ultimate addition and subtraction of counted events in phase with this modulation. This technique (analogous to the well-known cw phase-sensitive detection method) also provides cancellation in the experiment of background "noise." This background count is stored separately for the purposes of statistical analysis of the data. For clarity, a number of gating

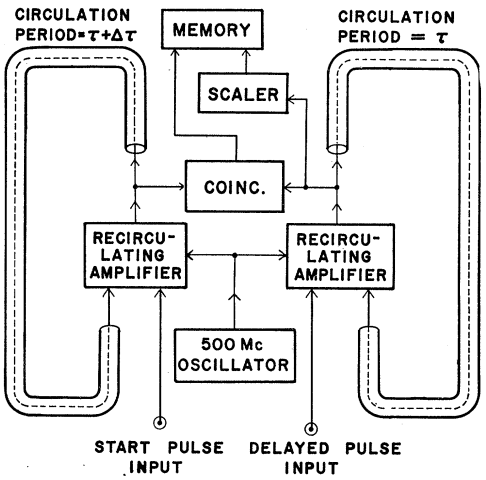

FIG. 2. Schematic diagram of the phase-locked vernier chronotron used to make the time interval measurements in the multichannel delayed coincidence analyzer.

[5] Reapplication of this same analogue method to a study of most of the levels in the $(2p)^5 3p$ configuration has recently been made by J. Z. Klose, Phys. Rev. 141, 181 (1966). Klose's data were taken considerably above threshold, however.

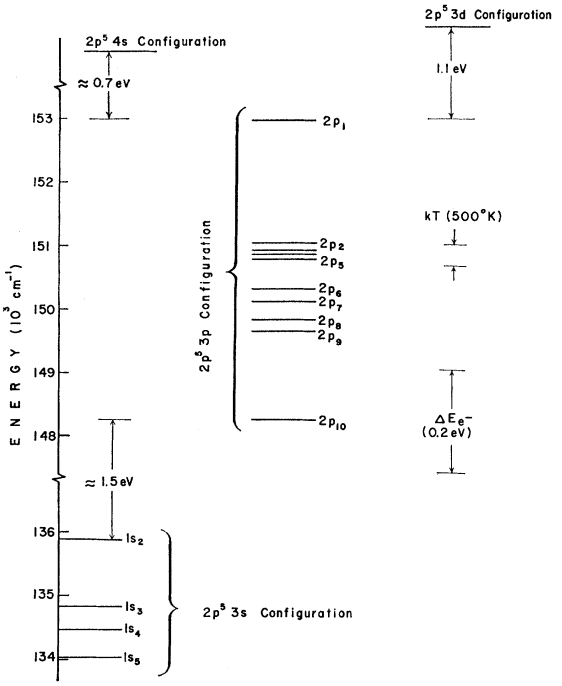

FIG. 3. Energy levels of atomic neon I pertinent to the present experiment.[7] The transitions studied are of the type $2p^53p \rightarrow 2p^53s$. The quantity kT at the gas temperature used in the experiment is indicated, along with the uncertainty in energy (ΔE_e), at the upper end of the electron energy distribution.

circuits and feedback stabilization loops have been omitted in Figs. 1 and 2. More detailed discussions of the circuitry are contained in Refs. 2 and 3.

The gun is part of a bakeable "ultra-high" vacuum system to which reagent-grade neon samples are admitted after further purification by storage in barium-coated flasks. The main initial impurity content in these samples consists of other noble gases at levels ≈ 10 parts per million (ppm). Pressures are measured with a capacitance manometer calibrated against an external mercurcy manometer and the gas temperatures are determined by taking the average of two thermocouple readings in planes bounding the region of excited gas. The measured rate of pressure increase in the sealed-off evacuated system under operating conditions is about 2×10^{-5} Torr per hour and data are taken over time intervals such that the background pressure never exceeds $\frac{1}{2}\,\mu$.

III. INTERPRETATIONAL CONSIDERATIONS

There are three main sources of interpretational difficulty in measurements of excited state lifetimes of the present type[1,2]: (a) resonance trapping, (b) radiative cascade, (c) excitation transfer in two-body collisions.

Because electric dipole radiation cannot occur from neon states in the $2p^53p$ configuration to the neon ground state, reabsorption of radiation emitted by these states could only occur on transitions to states in the excited $2p^53s$ configuration. Estimates based on the known electron flux, duty cycle, cross sections, metastable diffusion rates and Holstein's[6] theory show that the effects of process (a) are totally negligible for the present experimental conditions and range of A coefficients.

Effects of Radiative Cascade

The effects of radiative cascade have represented a serious limit to the accuracy of all previous studies of excited state lifetimes by other authors using electron impact which are known to us. In fact, it is nearly impossible in most previous work to make an accurate assessment of the limit of error introduced through process (b). The difficulty arises because of the (understandable) tendency of experimentalists to use excitation pulses near the peak of the excitation function for the transition, and hence, excitation pulses which are typically far above threshold for all other excited states in the atom or molecule. The transient decay of the level of interest, therefore, will generally contain a large number of exponential terms arising in radiative cascade from higher excited levels. The relative importance of these other exponential terms will, of course, depend on the electron excitation cross sections for the higher lying levels and on the pertinent oscillator strengths. The effect is apt to be smallest in the decay of states which are optically connected with the atom ground state because these states generally have the largest electron excitation cross sections far above threshold. However, with states [such as those in the neon $2p^53p$ configuration] having the same parity as the atom ground state, the electron excitation cross sections of higher lying states can be enormously greater than those of the level of interest, and order of magnitude errors can result from process (b). These errors can be eliminated by operation near enough to

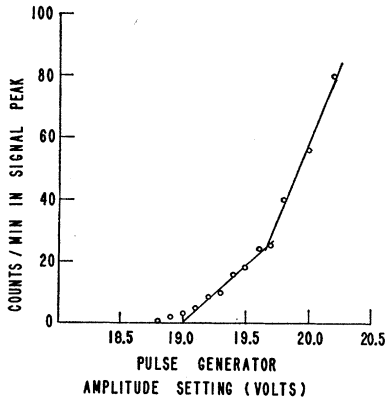

FIG. 4. Excitation function for the $2p_1$ state of neon seen under the conditions of the experiment. The sharp break in the excitation function above threshold is associated with radiative cascade from the $2p^54s$ configuration.

[6] T. Holstein, Phys. Rev. 72, 1212 (1947); 83, 1159 (1951).

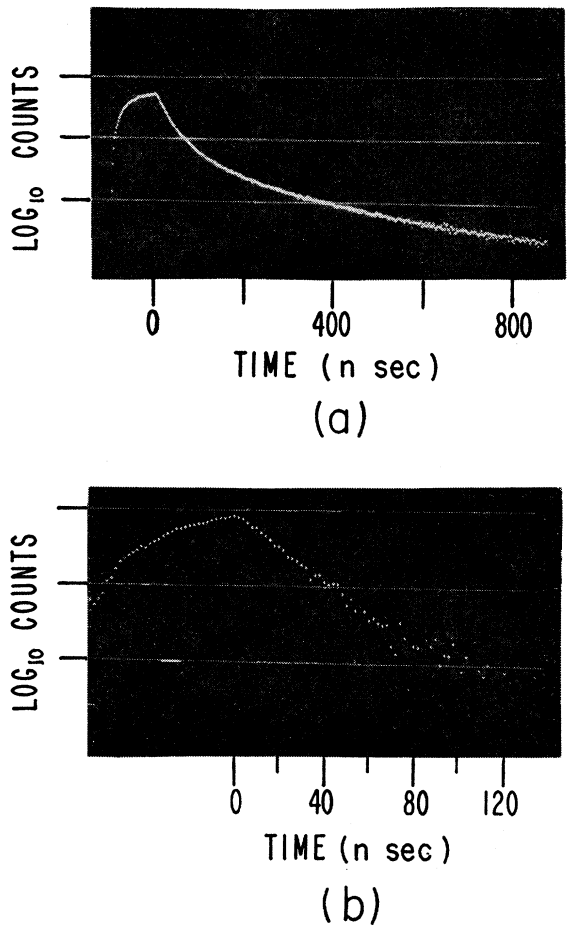

FIG. 5. Data taken on the $2p_2$ lifetime illustrating the effects of radiative cascade. The excitation pulse was turned off at time $t=0$ in each figure. The data in Fig. 5(a) correspond to an electron energy 11 eV above threshold and are characterized by more than 3 exponential decay terms. Fig. 5(b) was taken $\approx$0.1 eV above threshold and contained only one exponential component within the statistical accuracy. (See Fig. 6 and Table I.)

threshold so that cascade effects on optical transitions are eliminated.

Relevant energy levels for the present investigation are shown in Fig. 3, where it should be noted that a gap of $\approx$0.7 eV occurs between the uppermost level in the $2p^5 3p$ configuration and the next higher, optically connected states.[7,8] In the present experiment the excitation pulses were maintained within 0.1 to 0.2 eV above threshold for the particular level, as determined from the applied voltage pulse and checked against the individual appearance potential for the state. (See Fig. 4 and discussion in Ref. 2.)

The effects of cascade are illustrated in Figs. 5 and 6 with data taken on the $2p_2$ and $2p_8$ states at a pressure of 20 μ. Figures 5(a) and 6(a) show results obtained for an excitation pulse amplitude of 30 eV (about 11 eV above threshold), whereas the data in Figs. 5(b) and 6(b) correspond to threshold excitation. A summary of numerical analyses of these two sets of data is given in Table I. A least-squares analysis of the threshold data showed only one exponential decay in each case within the statistical accuracy of the data. Conversely, a least-squares analysis of the data taken at 30 eV indicated the probable existence of at least four significant exponential components. The results obtained from a forced reduction of the latter data to single, double, and triple exponential components are summarized in Table I, where an uncertainty equal to one standard deviation in the weighted least-squares analysis is indicated. The origin of previous order of magnitude errors in the measurement of the $3p$ lifetimes is obvious from the results in this table. However, the slow convergence of the fast decay rate towards the actual threshold value with increasing number of exponential components should also be emphasized. For example,

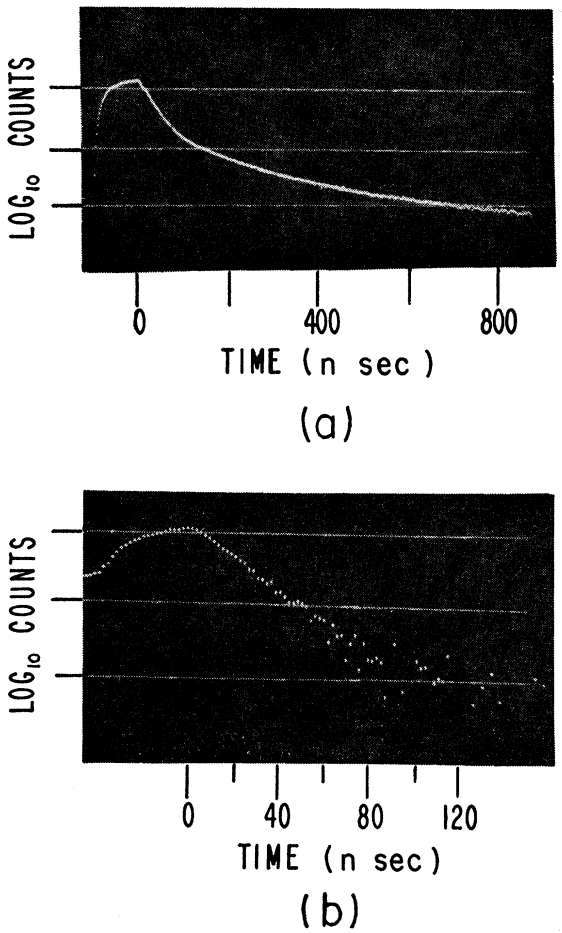

FIG. 6. Data taken on the $2p_8$ lifetime illustrating the effects of radiative cascade. Figure 6(a) corresponds to 11 eV above threshold and Fig. 6(b) corresponds to $\approx$0.1 eV above threshold. (See Fig. 5 and Table I.)

[7] *Atomic Energy Levels*, Edited by C. E. Moore, Natl. Bur. Std. (U. S.) Circ. No. 467 (U. S. Government Printing and Publishing Office, Washington, D. C., 1949), Vol. 1.

[8] Paschen notation will be used throughout the present paper as a convenient shorthand. The translation of this notation to that of *LS* and *jl* coupling is given in Table IV.

TABLE I. Comparison of typical lifetime data taken near and well-above threshold. The numbers listed represent inverse decay rates and are given in nsecs. The "uncertainty" quoted, in each case, is the weighted standard deviation for each exponential component in the least-square fit to the particular sum of exponentials indicated. All data correspond to a neon pressure of 0.02 Torr (see Figs. 5 and 6).

State (Paschen)	Threshold data 1 exponential[a]	11 eV above threshold 1 exponential	2 exponentials	3 exponentials
$2p_2$	18.7±0.3	59.2±1.3	28.2±0.3 154.6±1.8	25.2± 0.5 90.3±10 284 ±56
$2p_8$	19.7±0.2	52.3±1.2	29.0±0.1 158.8±1.4	27.4± 0.4 97.6±15 249 ±50

[a] No significant two-component reduction possible.

even with the three-component reduction of the 30-eV data for the $2p_2$ and $2p_8$ levels, the lifetime of the fast component still differs by more than ten times its standard deviation from the actual value obtained from the single component data taken at threshold energy. For these particular data, an evaluation of the $2p_2$ and $2p_8$ lifetimes from the multiple-component reduction would still have had undetermined errors of about 20 to 30%, and it seems clear that the only reliable method of evaluating the errors in such a multiple-component reduction consists in fact of retaking the data at threshold energy. It should be emphasized that the large number of exponential components required for a reasonable fit of the data taken at ≈11 eV above threshold is quite in keeping with the number of cascade transitions to be expected. For example, there are about a dozen strong transitions terminating in each of these levels from the next higher $2p^54s$ and $2p^53d$ configuration alone.

Effects of Inelastic Collisions

Because of the small fractional change in relaxation rates encountered due to collisions in the present work, the main purpose in considering collision processes here is to provide the basis for an objective means of correcting for systematic errors in the measured radiative relaxation rates due to collisions.

As described previously,[1,2] inelastic collisions can show up in the present type of experiment both through modification of the measured decay rates and by modification in the number of exponential decay components.

At low pressures, the transient decay of the ith level follows an exponential law of the type

$$n_i(t)=n_0\exp(-R_it), \tag{1}$$

with

$$R_i=\sum_j A_{ij}+n\sum_j\langle Vq_{ij}\rangle\equiv A_i+a_i, \tag{2}$$

where $\sum_j A_{ij}$ represents the total Einstein A coefficient for spontaneous decay for the level, the terms $\langle Vq_{ij}\rangle$ represent the velocity-averaged destructive collision rate with ground state atoms (density n) of state i through process j, and the total rate a_i increases linearly with the gas density. Numerically, the collision term ($a\equiv\alpha P$) is given by

$$a\equiv nvq=2.56\times10^6PQ(300/T)^{1/2}\ \text{sec}^{-1} \tag{3}$$

for neon-neon collisions, where P is the pressure in Torr, Q is in units of 10^{-15} cm^2, T is in °K, and the total velocity-averaged cross section (Q) may, of course, depend on the temperature. Because of the short radiative lifetimes, only two body collisions need be considered in the present experiment. Further, since the appearance potential for the reaction

$$\text{Ne}^*+\text{Ne}\rightarrow\text{Ne}_2^+ + e \tag{A}$$

has been established to fall well-above the $2p^53p$ configuration by Hornbeck and Molner[9], the only important inelastic collisions for this group are expected to represent excitation transfer in reactions of the type

$$\text{Ne}^*+\text{Ne}\rightarrow\text{Ne}+\text{Ne}^{**} \tag{B}$$

in which the difference in electronic energy between states Ne* and Ne** is exchanged with kinetic energy of the heavy particles. Such reactions generally have cross sections which are small compared with gas kinetic cross sections for energy differences much in excess of a few tenths of an eV,[10] but can have cross sections in excess of $\approx10^{-13}$ cm^2 for near coincidence of the two levels.[2] From the relative energy-level spacing in neon (see Fig. 3), it is very probable that the only important reactions of type (B) in the present work consist of transfer to other neighboring states in the $2p^53p$ configuration.[10] In this connection it should be noted that the final data for the lowest level in this configuration (the $2p_{10}$) exhibited an α_i coefficient which had a standard deviation from the pressure fit in excess of its probable value. As explained in Sec. V, even the average value might arise through endothermic collision to the $2p_9$. Hence, there is no evidence in the present work requiring a reaction of type (B) in which excitation is transferred out of the $2p^53p$ configuration.

At higher pressures, the effects of inelastic collisions can also introduce a departure from a pure single-component exponential decay. Multiple exponential components in the decay can arise both from collision cascade from higher lying levels (falling within the 0.1 to 0.2 eV spread at the high end of the electron-energy distribution) and from the effects of the inverse reaction to (B) in cases where kT is comparable to the difference in energy levels. We have studied this process in most

[9] J. A. Hornbeck and J. P. Molnar, Phys. Rev. **84**, 621 (1951).

[10] A possible exception might occur through "double crossings" with the intermediate ionic state, Ne^+-Ne^-, in the manner analyzed for atomic hydrogen collisions by D. R. Bates and J. T. Lewis, Proc. Phys. Soc. (London) **A68**, 173 (1955) and in Na–He collisions by J. H. Stamper and H. Margenau (to be published).

detail in the case of helium[2,11] where strong evidence of inverse transfer was obtained between P and D terms. The basic problem may be illustrated by considering the reciprocal transfer process shown schematically for two levels in Fig. 7. Here, the transient behavior of both levels is obtained through solution of the coupled equations

$$\begin{aligned}\dot{n}_1 &= -(A_1+a_1)n_1+a_{21}n_2,\\ \dot{n}_2 &= -(A_2+a_2)n_2+a_{12}n_1,\end{aligned} \tag{4}$$

where $a_1 \equiv a_{10}+a_{12}$ to allow for the inclusion of irreversible reactions in the term a_{10}, and similarly $a_2 \equiv a_{20}+a_{21}$. The solutions for the transient decay of both n_1 and n_2 are of the form

$$n = c_+e^{-R_+t}+c_-e^{-R_-t}, \tag{5}$$

where different coefficients ($c_\pm$) dependent on the boundary conditions are involved in the two states, but the *same* two decay rates,[1]

$$R_\pm = \tfrac{1}{2}(A_1+A_2+a_1+a_2) \pm [\tfrac{1}{4}(A_1-A_2)^2 + \tfrac{1}{2}(A_1-A_2)(a_1-a_2)+a_{12}a_{21}+\tfrac{1}{4}(a_1-a_2)^2]^{1/2} \tag{6}$$

occur in the transient decay of both excited state densities n_1 and n_2. As previously anticipated,

$$R_\pm \rightarrow \begin{cases} A_1+a_1 \\ A_2+a_2 \end{cases} \tag{7}$$

at low pressures. As the pressure increases, the collision process illustrated in Fig. 7 may result in a nonlinear dependence of the two decay rates on pressure. In the real case, more than two levels may of course be involved in the excitation transfer process, with the consequence that more than two exponential terms may be induced through collision effects in the transient decay.

When the exponential decay rates of the different levels are close in magnitude (as with most of the present levels), it is hard to obtain a meaningful resolution of the data into more than one exponential component without phenomenally high statistical accuracy. The low direct excitation cross sections we encountered in the $2p^53p$ configuration near threshold (as compared with excitation cross sections on "optically allowed" transitions from the neon ground state to the neighboring configurations) prevented us from obtaining the required statistical accuracy for a meaningful two-component reduction over the pressure range studied. Consequently, the only practical approach in the present experiment has been to fit the experimental data to a single exponential component. Here the effects of collision cascade and reciprocal transfer must be anticipated and show up through a nonlinear dependence of the apparent decay rate on pressure, and sometimes through an anomalous decrease of

[11] W. R. Bennett, Jr. and P. J. Kindlmann, Bull. Am. Phys. Soc. 8, 87 (1963).

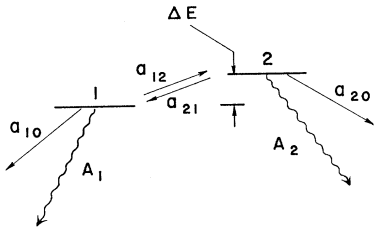

FIG. 7. Two-level model used to illustrate the effects of collision cascade and reciprocal collision transfer.

apparent decay rate with increasing pressure. It should be emphasized here that an important source of this nonlinear pressure dependence can arise through the forced reduction of a multiple component decay into a single exponential term, as opposed for example, to the inherent nonlinearity in Eq. (6). Final data extracted in the single component reduction is, of course, only meaningful in the linear pressure range;—or equivalently, only the first two terms in a power series expansion of the apparent decay rate may be given a direct physical interpretation.

IV. METHOD OF DATA ANALYSIS AND SUMMARY OF RADIATIVE LIFETIME MEASUREMENTS

For reasons outlined above, the data for each run were analyzed on the basis of a single exponential decay. Typically, each run (consisting of about 200

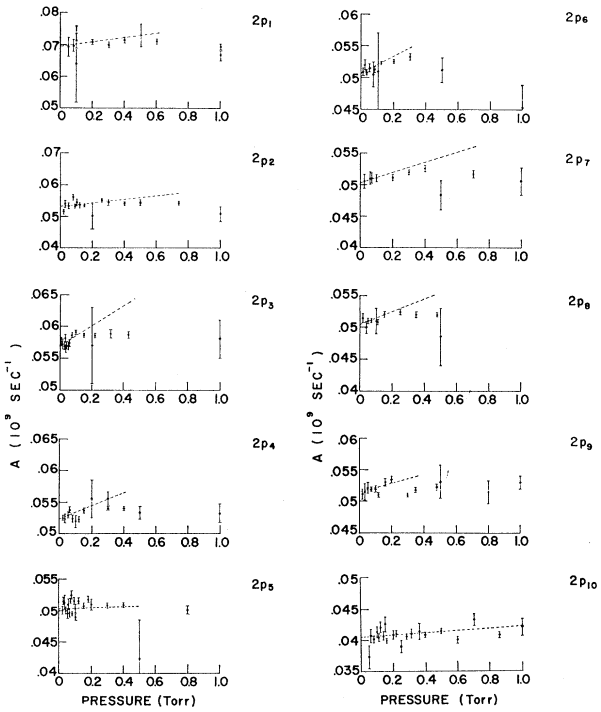

FIG. 8. Summary of experimental points used in the final pressure fits to determine the A coefficients and deactivation cross sections in the present work. The dashed line in each case represents the least square fit obtained for the first two terms in Eq. (8). The limits of error on the slope of the dashed line for the $2p_1$, $2p_5$, $2p_9$, and $2p_{10}$ are larger than the mean value.

TABLE II. Summary of final data. The values listed have been determined with a least-squares fit of the data to the form of Eq.(8). The pressure range and number of runs used for the final pressure fit are shown for each level. The errors quoted represent ± one standard deviation on the final pressure fit to Eq. (8). For each parameter, the spread of mean values encountered for all pressure fits (including runs at pressures higher than used in the final analysis) is given in parentheses.

State	A (10^7 sec^{-1})	α (10^7 sec^{-1} Torr^{-1})	β (10^7 sec^{-1} Torr^{-2})	Pressure (Torr)	No. of runs used
$2p_1$	6.95±0.13 (6.92 to 7.14)	+0.67±0.8 (−0.4 to +0.9)	−0.64±1.0 (−0.9 to +1.6)	0 to 0.6	8
$2p_2$	5.31±0.08 (5.31 to 5.39)	+0.52±0.52 (0 to 0.52)	−0.53±0.48 (−0.61 to 0)	0 to 0.75	17
$2p_3$	5.69±0.05 (5.61 to 5.80)	+1.6±0.6 (−1.4 to +8.8)	−3.0±1.2 (−11.0 to +34.0)	0 to 0.43	15
$2p_4$	5.23±0.08 (5.23 to 5.36)	+1.0±0.9 (−0.6 to 1.0)	−1.4±1.9 (−1.4 to +6.6)	0 to 0.40	11
$2p_5$	5.02±0.09 (5.02 to 5.07	+0.6±1.1 (0 to 0.65)	−1.2±3.0 (−1.2 to 0)	0 to 0.5	19
$2p_6$	5.07±0.05 (5.06 to 5.10)	+1.3±0.7 (0 to +1.6)	−1.6±2.3 (−2.6 to 0)	0 to 0.3	10
$2p_7$	5.03±0.09 (5.03 to 5.12)	+0.78±0.43 (0 to 0.78)	−0.83±0.52 (−0.83 to +0.89)	0 to 0.7	9
$2p_8$	5.04±0.05 (5.04 to 5.16)	+1.1±0.4 (−0.26 to +1.1)	−1.6±0.8 (−1.6 to +3.2)	0 to 0.5	11
$2p_9$	5.15±0.15 (5.01 to 5.26)	+0.7±2.0 (−0.4 to +2.7)	−2.2±4 (−6.5 to +1.4)	0 to 0.36	10
$2p_{10}$	4.04±0.06 (4.04 to 4.08)	+0.17±0.35 (−0.006 to +0.17)	−0.11±0.36 (−0.11 to 0)	0 to 1	21

separate data points at 2-nsec intervals in the transient decay) was analyzed using a least-squares analysis program by Rogers[12] which was modified for our specific needs (see Ref. 2). The standard deviation of the exponential decay rate is determined through this program from the individually weighted count of each channel in which allowance is made for the statistical variation in the photo detection multiplication process[13] (see Appendix). Runs were made on each of the 10 states in the $2p^53p$ configuration at approximately 20 different pressures, ranging from 0 to 10 Torr. The mean decay rates extracted from the least-squares analysis for each run are shown plotted in Fig. 8 together with their weighted standard deviations.

The decay rates obtained for each level were then fit to the power series

$$R=A+\alpha P+\beta P^2 \qquad (8)$$

using another least-squares program. As indicated above, the appearance of a significant quadratic term may be assumed to be associated with the appearance of a second exponential decay term which cannot be satisfactorily resolved because of statistical considerations. Consequently, the analysis of the data as a single exponential decay is not valid over the range where a significant quadratic term occurs. We therefore continued to reanalyze the data over a lower and lower pressure range until the standard deviation on the coefficient β was at least comparable to β. The coefficients of this final least-squares fit are listed in Table II, together with the various standard deviations, pressure range, and number of runs used in the final fit to Eq. (8). In each case enough additional runs were taken in the final "linear" region to result in a final "probable error" (0.67σ) of less than 2% in the determination of the A-values from the least-squares fit to Eq. (8). The A coefficients obtained in this manner are used to determine the final radiative lifetimes quoted in Table III, together with an "error" defined as the standard deviation in the final least-squares fit to Eq. (8). Also listed in parentheses in Table II are the maximum spread of the mean values of the coefficients A, α, and β encountered for all pressure fits made, including runs which were not used in the final analysis of the "linear region" and also including mean values for least-square fits to Eq. (8) when $\beta\equiv 0$ and when $\alpha\equiv\beta\equiv 0$. The coefficients α in Table II are identified with the velocity-averaged destructive cross sections and cannot be established with much less than about 50% error in the present experiment. The coefficients β in Table I may not be given any simple physical meaning and are used merely to define the linear pressure region and permit extraction of the linear coefficients in that region. It should be noted that in nearly all cases the extreme spread in mean values for the A coefficients is within one standard deviation of the final-pressure fit in the linear region. With levels such as the $2p_2$, $2p_3$, $2p_4$, $2p_6$, $2p_7$, and $2p_8$, which show a definite destructive cross section (or linear term) within the statistical uncertainty, the final A coefficient occurs close to the lower limit of the extreme spread. With

[12] P. C. Rogers, M. I. T. Laboratory for Nuclear Science, Technical Report No. 76 1962 (unpublished).
[13] A. Arcese, Appl. Opt. 3, 435 (1964).

TABLE III. Comparison with previously measured radiative lifetimes $1/A$ in nsec.

Level (Paschen)	Present work[a]	Klose[b]	Ladenburg[c]	Griffiths[d]	Osherovich and Petelin[e]	Doherty[f]
$2p_1$	14.4±0.3	14.7±1.3	<8	39± 2	51±2.5 46±2.5	28
$2p_2$	18.8±0.3	16.3±1.4	10.0±1	···		31
$2p_3$	17.6±0.2	23 ±6.6	12.5±1.1	···		31
$2p_4$	19.1±0.3	22 ±5.4	11.0±1	83±11	110±2.5	40
$2p_5$	19.9±0.4	18.9±2.8	<10.5	115±13	118±4	40
$2p_6$	19.7±0.2	22 ±3.2	13 ±1.5	91± 8	115±2.5	40
$2p_7$	19.9±0.4	20.3±2.6	13 ±1.5	···		37
$2p_8$	19.8±0.2	24.3±3.2	16 ±2	120±11	109±2	43
$2p_9$	19.4±0.6	22.5±3.1	17 ±2	200±30		34
$2p_{10}$	24.8±0.4	···	<10	···		59

[a] The errors quoted in the present work represent (±) one standard deviation on the final pressure fit to Eq. (8) and include allowance for all systematic" errors known to us to be present in the experiment.
[b] The errors on these measurements include "systematic" errors listed by Klose (Ref. 5) which are estimated from differential nonlinearities in his time analyzer and uncertainties in the radiative cascade contribution. Klose's values agree with ours within these "systematic" errors except for the $2p_2$ and $2p_8$ levels.
[c] R. Ladenburg, Rev. Modern Phys. **5**, 243 (1933).
[d] J. H. E. Griffiths, Proc. Roy. Soc. (London) **143**, 588 (1934); **147**, 547 (1934).
[e] A. L. Osherovich and G. M. Petelin, Dokl. Akad. Nauk SSSR **129**, (1959) [English transl.: Soviet Phys.—Doklady **4**, 1289 (1960)].
[f] L. R. Doherty, Ph.D. thesis, University of Michigan, 1962, p. 154 (unpublished).

levels such as the $2p_1$, $2p_5$, $2p_9$, $2p_{10}$ which show no significant cross section (i.e., the standard deviation of α is greater than the mean), the A coefficient is not as depressed towards the lower limit of the extreme spread. The upper limits on the cross sections for the latter cases have been determined from the upper limits on the extreme range of the α coefficients given in Table II. It should be emphasized that this analysis has included allowance for all systematic effects on the radiative lifetimes known to us to exist. The final error on the A values derived in the above way is therefore an objective evaluation of the total error in the experiment and should be regarded as such within the usual statistical "confidence factors" (e.g., 68% for 1 standard deviation, etc.).

Individual A Coefficients for the $3p \rightarrow 3s$ Transitions of Neon

Relative values for line strengths of the $3p \rightarrow 3s$ transitions of neon have been obtained previously through dispersion measurements by Ladenburg,[14] through absorption measurements by Krebs,[15] Dixon and Grant,[16] and Phelps,[17] and through intensity measurements by Dorgela[18] and Garbuny.[19] A convenient summary of relative line strengths based on the most reliable absorption[15] and emission[19] data has been prepared by Phelps[17] in which comparisons are made with the J-file sum rules of Shortley.[20] Phelps also has presented a table of relative line strengths based on a statistical average of these emission and absorption data, which in turn probably represent the best averaged experimental values available. We have used these averaged relative-line-strength data (Table VII of Ref. 17) to obtain the individual A coefficients in Table IV by normalizing the sum of the calculated relative A coefficients for each upper state against our measured values for the total radiative-decay rates. (In preparing Table IV, a correction for the wavelength-cubed factor has, of course, been made.) The limits of error for the individual A coefficients obtained in this manner are difficult to assess and clearly will be large compared to our measured limits of error on the total radiative decay rates (typically about 2%). Some estimate of the errors expected can be made from the consistency obtained for the individual A coefficients when the different sets of relative-line-strength data summarized by Phelps are used separately. Such a comparison showed that most of the A coefficients obtained separately from the two sets of data were consistent within about 10 to 20%. As noted in Table IV, however, two instances were encountered in which these discrepancies were as much as ≈50%. A similar range in discrepancies was found by Phelps in the comparison of the experimental line strengths with J-file sum rules. There, the agreement was typically good to about 10 to 20%. However, the J-file sum for the $1s_2$ level was anomalously large by about 30 percent. These values for the individual A-coefficients in Table IV are used in the next section to evaluate the radial part of the $3p \rightarrow 3s$ transition probability.

Radial Part of the Transition Probability

The spontaneous electric dipole transition probability for the transition $(i \rightarrow f)$ may be written in the central-field approximation as

$$A_{if}=\frac{64\pi^4}{3h\lambda^3}\frac{S(i,f)}{(2J_i+1)}=\frac{2.026\times10^{18}}{\lambda^3(\text{Å})}\frac{\mathcal{S}(\mathfrak{M})\mathcal{S}(\mathfrak{L})}{(2J_i+1)}\sigma^2\,\text{sec}^{-1}, \quad (9)$$

where the numbers in the second expression are evalu-

[14] R. Ladenburg, Rev. Mod. Phys. **5**, 243 (1933).
[15] K. Krebs, Z. Physik **101**, 604 (1936).
[16] J. R. Dixon and F. A. Grant, Phys. Rev. **107**, 118 (1957).
[17] A. V. Phelps, Phys. Rev. **114**, 1011 (1959).
[18] H. G. Dorgela, Physica **5**, 90 (1925).
[19] M. Garbuny, Z. Physik **107**, 362 (1937).
[20] G. H. Shortley, Phys. Rev. **47**, 295 (1935).

TABLE IV. Individual A-coefficients for the $2p^5 3p \rightarrow 2p^5 3s$ transitions of neon determined from averaged emission and absorption relative line-strength data (see text) and the total radiative decay rates measured in the present work. Except where noted, the consistency of separate determinations of the individual A coefficients from the different relative line-strength data was good to ≈ 10 to 20%. For convenience, state designations are given in LS, Racah, and Paschen notation. The values are in units of 10^7 sec^{-1}. *Note added in proof.* We are indebted to Dr. A. V. Phelps for calling our attention to measurements of a number of these transition probabilities made by A. Pery-Thorne and J. E. Chamberlain [Proc. Phys. Soc. (London) **82**, 133 (1963)] with the anomalous dispersion method. The values of Pery-Thorne and Chamberlain are generally in much closer agreement with our data than the earlier anomalous dispersion measurements by Ladenburg and typically agree within the estimated errors ($\approx$30%). The few instances where larger discrepancies exist do not indicate any obvious systematic effects.

LS	Racah	Paschen	$3s\,{}^3P_2^\circ$ $3s[3/2]_2^\circ$ $1s_5$	$3s\,{}^3P_1^\circ$ $3s[3/2]_1^\circ$ $1s_4$	$3s\,{}^3P_0^\circ$ $3s'[1/2]_0^\circ$ $1s_3$	$3s\,{}^1P_1^\circ$ $3s'[1/2]_1^\circ$ $1s_2$	Measured total A coefficient
$3p\,{}^1S_0$	$3p'[1/2]_0$	$2p_1$	0	0.07[a,b]	0	6.88	6.95
$3p\,{}^3P_1$	$3p'[1/2]_1$	$2p_2$	0.82[a]	0.48[a]	1.53[c]	2.49[b,c]	5.32
$3p\,{}^3P_0$	$3p[1/2]_0$	$2p_3$	0	5.60	0	0.09[a,b]	5.69
$3p\,{}^3P_2$	$3p'[3/2]_2$	$2p_4$	0.90[a]	1.56[a]	0	2.77[b]	5.23
$3p\,{}^1P_1$	$3p'[3/2]_1$	$2p_5$	0.31[a,b]	0.05[a,b]	2.27[b]	2.38	5.02
$3p\,{}^1D_2$	$3p[3/2]_2$	$2p_6$	2.31[b]	0.45[b]	0	2.31[a]	5.07
$3p\,{}^3D_1$	$3p[3/2]_1$	$2p_7$	0.52	3.03	1.19[a]	0.30[a,b]	5.03
$3p\,{}^3D_2$	$3p[5/2]_2$	$2p_8$	1.64	2.89	0	0.51[a,b]	5.04
$3p\,{}^3D_3$	$3p[5/2]_3$	$2p_9$	(5.15±0.15)	0	0	0	5.15
$3p\,{}^3S_1$	$3p[1/2]_1$	$2p_{10}$	2.44	1.01	0.30[a]	0.30[a,b]	4.04

[a] Transition forbidden in jl-coupling.
[b] Transition forbidden in LS-coupling.
[c] Indicates cases where discrepancies $\approx$50% arose from determinations based on relative line-strength data obtained separately from absorption and emission data.

ated for λ in Å and σ^2 in atomic units. The angular factors, $\mathcal{S}(\mathfrak{M})$ and $\mathcal{S}(\mathfrak{L})$, depend on the particular multiplet, line within the multiplet and coupling scheme, and are available from tables in the literature.[21]

The radial part of the electric dipole transition probability is contained in the factor,

$$\sigma^2 \equiv \frac{1}{4l_>^2-1}\left(\int_0^\infty R_i R_f r\, dr\right)^2, \tag{10}$$

where $l_>$ is the greater of the two azimuthal quantum numbers involved in the transition.

The reduction of the line strengths, $S(i,f)$ in Eq. (9), into the products of relative angular factors and a common radial factor for the $3p \rightarrow 3s$ transitions is valid so long as the same configurations are involved in all transitions. In this limit we may use the J-file sum rules of Shortley[20] to evaluate σ^2 from our data in a manner independent of the actual coupling scheme. Shortley has shown for the $p \rightarrow s$ transitions of neon under consideration that $\sum_s S(p,s) = (2J_p+1)\Xi(p,s)$ where the factor $\Xi(p,s)$ is independent of the coupling scheme and depends only on the two configurations involved. The latter sum rule is particularly useful because of the uncertainties in the actual coupling scheme involved. (e.g. There are a large number of transitions listed in Table IV which would be forbidden in any of the commonly assumed coupling schemes.) Hence, by evaluating $\Xi(p,s)$ in the LS couping scheme, we may obtain a separate determination of σ^2 for each of the upper states observed. Hence, for each state in the $3p$ configuration we obtain

$$\sigma_p^2 = (3h/64\pi^4)\sum_s(\lambda_{ps}{}^3 A_{ps}). \tag{11}$$

A similar sum rule,

$$\sigma_s^2 = \left(\frac{h}{64\pi^4}\right)\sum_p \frac{(2J_p+1)\lambda_{ps}{}^3 A_{ps}}{(2J_s+1)} \tag{12}$$

may be written for the sum over the p states for each s state. However, it should be noted that the quantity directly measured in the present experiment is

$$A_p = \sum_s A_{ps} \tag{13}$$

for each p state. Consequently, a much more accurate evaluation of σ^2 may be obtained from Eq. (11) than from Eq. (12) with the present data. In Eq. (11), the errors in the relative line strength determination only enter through differences in the λ^3 factor and cancel to a large extent. In Eq. (12) there are not only many more transitions to sum over, but also the errors in σ^2 introduced by the relative-line-strength errors are additive in the present normalization procedure. Values of σ^2 determined from Eq. (12) in the present case in fact were found to differ by as much as 50% from those obtained from Eq. (11). It is possible that some of these discrepancies may also be attributable to the same causes that produce the inconsistencies in σ^2 described below.

Values of σ^2 determined from Eq. (11) and the data in Table IV are summarized in Table V. It is difficult to make a quantitative estimate of the errors in σ^2 due to relative line-strength inaccuracies in cases where more than two transitions start in the same upper state, except to note that they will generally tend to be smaller than the fractional discrepancies encountered

[21] B. W. Shore and D. H. Menzel, Astrophys. J. Suppl. **12**, 187 (1965) have a complete compilation of the required factors; the appendix to this paper also has a convenient translation of notation between various previous papers on this subject.

in the individual line strengths. Consequently, we have only quoted limits of error on values of σ^2 determined from the $2p_9$, $2p_3$, and $2p_1$ states. With the $2p_9$, only one transition is involved. In the other cases we made independent relative intensity measurements in order to set an upper limit on the final errors. Although most of the values of σ^2 listed in Table V are consistent well within the 10 to 20% discrepancies in the relative line-strength data, the result for the $2p_3$ definitely falls below the other "precision" determinations by more than the combined limits of error and the value for the $2p_{10}$ appears anomalously high. About the only obvious factors common to the $2p_3$ and $2p_{10}$ levels which are not shared with the others in the $3p$ configuration are that they comprise the only jl-coupling pair with the same core and K values which are both widely spaced and separated by several other levels.

If there were no significant variation of σ^2 over the transitions between these configurations, one would of course adopt the value (6.67±0.2 a.u.) obtained from the $2p_9$ lifetime as the most accurate determination since only one transition is allowed from the upper state and the measurement is clearly independent of all relative-line-strength data. There does seem to be a definite indication of a small (≈5%) but real variation in σ^2 between the most accurately determined values, however.

A possible cause of the observed discrepancies in σ^2 is configuration interaction. We can do no more here than make a very rough estimate of the magnitude of the effect to be expected. Neither the selection rules nor the interval rules for any of the commonly assumed coupling schemes are closely obeyed in the states of neon under consideration. It may also be that different coupling schemes should be considered in the two configurations. However, it is to be expected that the dominant interactions will be contained in the Hamiltonian leading to the fine structure splitting in terms such as

$$H'=f(r)[\mathbf{j}\cdot\mathbf{l}], \tag{14}$$

where $f(r)$ represents a radial factor and the particular angular-momentum factors depend on the actual coupling scheme. From the magnitude of the fine-structure splitting, $\langle R_{3p}(\mathrm{J})|H'|R_{3p}(\mathrm{J})\rangle$ must vary by amounts ≈1000 cm^{-1} for the different angular-momentum states in the $2p^53p$ configuration. Similarly, mixing of the other p configurations will occur with the $3p$ of an amount given by[22]

$$R_{3p}'(\mathrm{J})\approx R_{3p}-\sum_n \frac{\langle R_{np}(\mathrm{J})|H'|R_{3p}(\mathrm{J})\rangle}{E_{np}-E_{3p}}, \tag{15}$$

where the coefficients in the sum will vary with the different angular-momentum states in the configuration. Because of its proximity, the main terms in the sum in Eq. (15) will be from the $4p$ configuration, for which $E_{4p}-E_{3p}\approx 12\,000$ cm^{-1}. Although we do not know either the factors $f(r)$ or the radial wave functions, for the purpose of rough estimate it is expected that $\langle R_{4p}(\mathrm{J})|H'|R_{3p}(\mathrm{J})\rangle\approx\langle R_{3p}(\mathrm{J})|H'|R_{3p}(\mathrm{J})\rangle$. Consequently, a mixing of the $2p^54p$ configuration with the $2p^53p$ would be expected which varied over the fine structure levels by amounts up to ≈8% on the probability amplitude. This mixing would introduce a roughly comparable variation in σ^2 for the observed transitions. Although the estimate is extremely approximate, it nevertheless indicates that configuration interaction could introduce variations in σ^2 of about the magnitude observed. It also seems likely that the same phenomenon would help explain the discrepancies with the sum rules previously found in the relative emission and absorption data.[17] Unfortunately, the present data are not accurate enough to determine whether there is a definite correlation of these variations in σ^2 with a particular coupling scheme.

TABLE V. Values of σ^2 determined from the total radiative decay rates measured in the present work, the previous relative line-strength data used to compile Table IV, and the sum rule expressed in Eq. (11).

Upper state	σ^2 (in atomic units)
$2p_1$	(6.86±0.2)
$2p_2$	6.6
$2p_3$	(6.32±0.2)
$2p_4$	6.7
$2p_5$	6.7
$2p_6$	7.0
$2p_7$	6.6
$2p_8$	6.9
$2p_9$	(6.67±0.2)
$2p_{10}$	7.4

Comparison with the Coulomb Approximation

Bates and Damgaard[23] noted that the potential in the central-field approximation closely reached its asymptotic form before the region was reached in transitions involving excited states of lighter atoms which gave the dominant contribution to the integral in Eq. (10). Since the tables developed by Bates and Damgaard[23] are particularly convenient for the rapid evaluation of the radial matrix elements, it is of interest to compare values of σ^2 determined from the Coulomb approximation with those based on the present measurements. In this connection it should be noted that few previous measurements of transition probabilities have been made with an accuracy sufficient to show up the failure of this approximation.

The binding-energy parameters E_{nl} required to determine σ^2 in the method of Bates and Damgaard are most appropriately obtained from the binding energy of the center of gravity of each configuration

[22] This type of analysis of configuration mixing was first given in the case of cesium by E. Fermi, Z. Physik **59**, 680 (1929).

[23] D. R. Bates and A. Damgaard, Phil. Trans. Roy. Soc. A242, 101 (1950).

TABLE VI. Summary of total deactivation cross sections.

State (Paschen)	Cross section (in 10^{-15} cm^2) (at 500°K)	a_{ij}/a_{ji} (from data) for adjacent levels	(g_j/g_i) $\times\exp[-(E_j-E_i)/kT]$ (for 500°K)
$2p_1$	3.3± 4[a]	>0	0.001_4
$2p_2$	2.6± 2.6	>1.0	2.1
$2p_3$	8 ± 3	0.04 to 1.9	0.17
$2p_4$	5 ± 4.5	0 to 3.5	1.3
$2p_5$	3 ± 5.5[a]	>0.35[b]	0.16
$2p_6$	6.5± 3.5[c]	0.2 to 2	0.96
$2p_7$	3.9± 2.2	0.57 to 4.4[b]	0.26
$2p_8$	5.5± 2[c]	0 to 3.8	0.44
$2p_9$	3.5±10[a]	>0	0.04
$2p_{10}$	0.4± 1.7[a]		

[a] No significant cross section indicated by the present measurements.
[b] Denotes cases where reciprocal collisions between a pair of adjacent levels may be ruled out by the data as being a dominant destruction process, i.e. the measured range in a_{ij}/a_{ji} does not include $(g_i/g_i)\times\exp[-(E_i-E_i)/kT]$.
[c] Data imply that cross section is for an exothermic collision only.

[i.e., $\sum E_J(2J+1)/\sum(2J+1)$] since the fine-structure separations are associated with the interaction of the orbital and spin momenta. Thus we obtain $\bar{E}=23\,994.0$ cm^{-1} for the $2p^5 3p$ configuration and $\bar{E}=39\,517.2$ cm^{-1} for the $2p^5 3s$ configuration. These energy parameters lead to values of $\mathfrak{F}=3.50$ and $\mathfrak{g}=0.735$ for the interpolated values of the two functions tabulated by Bates and Damgaard, and finally to the value

$$\sigma_{\text{calc}}{}^2=6.62 \text{ atomic units}, \tag{16}$$

which is in astonishingly good agreement with the values determined experimentally in Table V. Equation (16) falls within the experimental error ($\approx 3\%$) of the most accurately determined value in Table V and the only significant discrepancies also represent internal discrepancies in the constancy of σ^2 over the different transitions between these two configurations. As discussed above, these discrepancies may very well have their origin in configuration interaction.

V. INELASTIC COLLISION CROSS SECTIONS

A summary of velocity-averaged total destructive cross sections is given in Table VI. These cross sections have been determined from the coefficients in Table II and the assumption of a Maxwellian velocity distribution at the measured gas temperature in the excitation region (300±20°K). [See Eqs. (2), (3) and associated discussion.] Only very approximate values can be obtained for these inelastic cross sections because of the large standard deviation in the linear pressure coefficients. It should be emphasized, however, that the reason for these large uncertainties is not that the cross sections themselves are small. They appear, in fact, to be comparable to normal gas kinetic cross sections in most cases. The inaccuracy arises primarily from the inability to resolve the multiple component decays which result from collisions at higher pressures. As previously discussed, this inability to analyze the data as a sum of exponential terms is due to the near coincidence in the actual values of the different decay rates present in the data.

For the $2p_1$, $2p_5$, $2p_9$, $2p_{10}$ levels $\alpha>0$, but the standard deviation in the cross section was larger than the mean. For the other levels, the observed cross sections show a rough inverse correlation with the spacing of adjacent levels, as might generally be expected for the behavior of collisions of the type

$$\text{Ne}^*+\text{Ne}\rightarrow\text{Ne}^{**}+\text{Ne}$$

in which excitation is transferred from one excited state to another.

Although the limits of error on these cross sections are of necessity quite crude, one further rough check on the nature of the collision process may be made. If we assume that all excited atoms observed in the experiment have the same Maxwellian velocity distribution at temperature T, it follows from detailed balancing that the individual transfer rates between a pair of levels of the type indicated in Fig. 7 should be related by

$$a_{12}=a_{21}(g_2/g_1)e^{-(E_2-E_1)/kT}, \tag{17}$$

where the g's are the statistical weights of the levels and E_2, E_1 are the two internal energies. One may then examine the various pairs of levels for evidence of reciprocal transfer. Such a comparison has been made in Table VI for pairs of adjacent levels in the $2p^5 3p$ configuration. As may be seen from this comparison, there are actually only a few instances in which reciprocal transfer between two adjacent levels may be ruled out on the basis of the data as being a dominant inelastic process. In particular, even the range in destructive cross sections for the $2p_{10}$ might be explained by endothermic transfer to the $2p_9$ within the accuracy of the data, as opposed, for example, to transfer to states in the $2p^5 3s$ configuration 1.5 eV below. For many levels, it is of course to be expected that collision cascade will be more important in this configuration. However, there is no indication in the present data that any collision process other than excitation transfer within the $2p^5 3p$ configuration is needed to explain our results.

VI. LASER CONSIDERATIONS

Nearly all of the important laser transitions in the helium-neon system terminate in the neon configura-

tion studied here.[24] The data presented in Table II should be sufficient to determine the total contribution of inelastic relaxation processes in these levels to the phase interruption widths on the important laser transitions to within $\approx 2\%$ for the pressure conditions typically used. The present data, of course, do not include the effects of elastic collisions. However, the large-angle elastic-scattering cross sections are apt to be of roughly the same magnitude as the inelastic cross sections determined here and, since the pressure effects due to neon-neon collisions are a small fraction of the total lower state relaxation rate, a reasonably accurate allowance for elastic collisions may be made by doubling the linear pressure coefficient term in Table II. For example, the $2p_4$ state is a common lower level for a number of important laser transitions. For an operating pressure of 0.1 Torr and temperatures comparable to the present ones, our data would imply a total phase interpretation rate $\approx 5.4\times 10^7$ sec^{-1}. This number would contribute ≈ 8.6 Mc/sec to the non-power-broadened Lorentzian width and, for example, would correspond to that part of the "hole" burned in the population distribution near threshold due to lower state relaxation processes involving neon atoms alone.[25] Additional contributions to these phase interruption widths will also arise due to the effects of helium-neon collisions on the lower state and from the upper state relaxation processes. Although some data has been reported on the relaxation rates of the upper laser levels in the limit of complete resonance trapping,[1] the most important upper state phase interruption processes in many cases are due to vacuum ultraviolet transitions to the atom ground state which have still not been studied directly.

The Transiently-Inverted Green Neon Laser

Leonard *et al.*[26] have recently reported pulsed oscillation on the $2p_1 \rightarrow 1s_4$ transition of neon at 5401 Å which appears to be inherently transient in character. They refer to this line as a strong, allowed transition of neon and found that the oscillation was self terminating in an interval ≈ 5 nsec. They were unable to obtain similar oscillation on any of the other $3p \rightarrow 3s$ transitions. Because of the short time delay (≈ 2 nsec) between the discharge pulse and laser emission pulse, Leonard *et al.*[25] have suggested that the main excitation process consists simply of direct excitation from the neon ground state in the reaction

$$e + \mathrm{Ne} \rightarrow \mathrm{Ne}(2p_1) + e \qquad \text{(a)}$$

and refer to measurements by Druyvesteyn and Penning[27] as supporting the notion that an inversion would occur on the $2p_1 \rightarrow 1s_4$ transition due to the relative cross sections for reactions (a) and the reaction

$$e + \mathrm{Ne} \rightarrow \mathrm{Ne}(1s_4) + e. \qquad \text{(b)}$$

They also note that the Born approximation can give erroneous values for relative excitation cross sections near threshold and argue that such an error would be introduced in estimating the relative cross sections in reaction (a) and reaction (b). Since reaction (b) represents an "optically allowed" transition and reaction (a) does not, the Born approximation would normally predict a larger cross section for reaction (b) than for (a) and would therefore suggest that a transient inversion on the $2p_1 \rightarrow 1s_4$ transition would not occur through reactions (a) and (b) alone.

Since it is not entirely clear that our results support the interpretation given by Leonard *et al.*,[26] it is worth summarizing some of the relevant observations. First of all, it is difficult to see how any meaningful relative excitation cross sections for reactions (a) and (b) can be obtained out of the discharge data reported in Ref. 27. It is clear that multiple step processes will become very important in exciting the $2p^5 3p$ configuration in the conditions described in Ref. 27 and it is not obvious how these may be unscrambled from the direct reactions (a) and (b). Second, the excitation function data taken in the present work (see Fig. 4; also see Fig. 3 of Ref. 1) are actually in reasonably good qualitative agreement with the relative cross sections predicted by the Born approximation, even *near* threshold. We have not, of course, looked at the excitation function for the $1s_4$ level. However, there is no evidence of significant structure in the $2p_1$ cross section near threshold. At the same time the excitation function for that level clearly implies that cascade contributions from higher levels that *are* optically connected with the neon ground state are much more important in populating the $2p_1$ than process (a) at energies in excess of ≈ 20 eV. The same conclusion is supported by the lifetime data taken appreciably above threshold (see Figs. 5 and 6 and associated discussion). Similarly, the relative excitation cross sections for the $2p^5 4s$ and $2p^5 3p$ configurations have been found to be such as to support cw oscillation on transitions of the type $2s_{2,4} \rightarrow 2p$ in low pressure discharges containing pure neon. It is certainly true, however, that the 2 nsec time delay encountered between the discharge pulse and laser output pulse is not compatible with the lifetimes measured for the important cascade contributions to the $2p_1$ from the higher states that are optically connected to the neon

[24] See, W. R. Bennett, Jr., Appl. Opt. Suppl. **2**, 3 (1965) for a recent compilation of these transitions and a discussion of the collision processes involved.

[25] For related theoretical discussions, see: W. R. Bennett, Jr., Phys. Rev. **126**, 580 (1962); Appl. Opt. Suppl. **1**, 24 (1962) and **2**, 3, 78 (1965); W. R. Bennett, Jr., in *Quantum Electronics*, edited by P. Grivet and N. Bloembergen, (Columbia University Press, New York, 1964), pp. 441–458; W. E. Lamb, Jr. and T. M. Sanders, Phys. Rev. **119**, 1901 (1960); W. E. Lamb, Jr., *ibid.* **134**, A1429 (1964); A. Szöke and A. Javan, Phys. Rev. Letters **10**, 521 (1963).

[26] D. A. Leonard, R. A. Neal, and E. T. Gerry, Appl. Phys. Letters **7**, 175 (1965).

[27] M. J. Druyvesteyn and F. M. Penning, Rev. Mod. Phys. **12**, 87 (1940).

ground state. Consequently, if the interpretation in Ref. 26 is correct, it seems probable that the inversion is obtained because the cross section for reaction (b) is anomalously *low* for an optically connected level, rather than that the the cross section for reaction (a) is anomalously high for a state with the same parity as the neon ground state. In that regard, it should be noted that the $1s_4$ level would not be optically connected with the atom ground state if LS coupling held strictly in the $2p^5 3s$ configuration.[28]

There are other characteristics of the problem which are worth noting. In contrast to being a strong transition, the A-coefficient ($\approx 7\times 10^5$ sec^{-1}) for the $2p_1 \rightarrow 1s_4$ transition appears in fact to be the smallest for any of the $2p^5 3p \rightarrow 2p^5 3s$ transitions which are not strictly forbidden by the selection rules on ΔJ (see Table IV). This characteristic of the transition would certainly at least contribute to the selective build up of a population inversion on the $2p_1 \rightarrow 1s_4$ transition over others of the $3p \rightarrow 3s$ under the conditions reported in Ref. 25.

Another process which also should at least be considered in the above case consists of stepwise excitation in successive reactions of the type

$$e+\mathrm{Ne} \rightarrow \mathrm{Ne}(2p^5 3s)+e \qquad \text{(c)}$$

and

$$e+\mathrm{Ne}(2p^5 3s) \rightarrow \mathrm{Ne}(2p^5 3p)+e. \qquad \text{(d)}$$

Evidence of the importance of these reactions has been obtained in cw rf discharges in pure neon.[24] It is also not obvious that such stepwise processes can be ruled out on the basis of the time delays alone in the experiments in Ref. 26. That is, for the electron densities typically involved in high-current discharges of the type reported in Ref. 26 and realistic estimates of electron excitation cross sections, it is not implausible that two-step processes such as (c) and (d) could build up a superradiant population inversion in a few nsec. It is of interest to note which excited states might be expected to predominate in such a two-step reaction on the basis of the Born approximation. The strongest resonance line from the neon ground state would be to the $1s_2$ state in the limit that LS coupling is at least partially obeyed in the $2p^5 3s$ configuration. Consequently, the largest electron excitation cross section through reaction (c) would be expected for production of the $1s_2$ level. From Table IV, the largest A coefficient from the $1s_2$ is, in fact, to the $2p_1$. Consequently, a two-step process through the $2p^5 3s$ configuration of the type

$$\begin{aligned} e+\mathrm{Ne} &\rightarrow \mathrm{Ne}(1s_2)+e \\ e+\mathrm{Ne}(1s_2) &\rightarrow \mathrm{Ne}(2p_1)+e \end{aligned} \qquad \text{(e)}$$

would be expected to be dominant on the basis of the Born approximation and would indeed lead to preferential excitation of the $2p_1$. Although the relative line strengths (obtained by multiplying the A coefficients in Table IV by the wavelength-cubed factors) would be more appropriately used in the estimate, the largest strength from the $1s_2$ is still to the $2p_1$, by an amount $\approx 50\%$ more than any of the others.[29] In summary, although more experimental data are obviously needed to determine the actual excitation processes involved in the pulsed $2p_1 \rightarrow 1s_4$ laser, it is far from clear that use of the Born approximation to estimate the relative cross sections in this instance has been demonstrated to lead to wrong results.

[28] *Note added in proof.* The calculated oscillator strength for transitions from the $1s_2$ and $1s_4$ states to the neon ground state are in the ratio of about 10:1. [See, A. Gold and R. S. Knox, Phys. Rev. **113**, 834 (1959).]

ACKNOWLEDGMENTS

The authors are indebted to B. Wexler and J. Hines for help in the numerical analysis of the data. We are particularly indebted to D. MacNair for help in preparing the cathode used in the electron gun, to E. Brosius and H. Vander Gouw for glass blowing assistance, to A. Valentino for technical assistance and to the Bell Telephone Laboratories for the grant of some of the apparatus used in the experiment. It is also a pleasure to acknowledge helpful discussions with G. N. Mercer, C. J. Elliott, and Dr. E. A. Ballik.

APPENDIX

As has been noted by Arcese,[13] random variations in the photoelectron multiplication process result in effective signal-to-noise ratios from photomultiplier tubes that can be appreciably worse than $\sqrt{n_0}$, where n_0 is the mean number of photons striking the photocathode in the observation time. Although his result applies in the case where a continuous output waveform is derived from the multiplier current and is used to measure the average photon flux, the result may also be used to estimate the effective signal-to-noise ratios obtained in the present experiment. Arcese's derivation involves the specific nature of the distribution function and is not the most transparent way to obtain the final answer for the signal-to-noise ratio. We therefore give a simpler, more physical derivation here.

Let the total number of electrons (including all secondaries) arriving at the last dynode of the photomultiplier during the observation time be

$$n=n_0\eta_e\eta_1\cdots\eta_n, \qquad \text{(A1)}$$

where n_0 is the mean number of photons incident on the cathode, η_e is the mean photo-detection efficiency of the cathode, η_1 is the mean electron-multiplication factor of the first dynode, and η_n is the mean multiplication factor of the last dynode. In the continuous-wave case,

[29] *Note added in proof.* V. P. Chebotayev and I. Beterov (private communication) have made measurements of the relevant cross sections which apparently do indicate that reactions (*e*) represent the dominant two-step excitation process for the $2p^5\ 3p$ configuration and would lead to a transient population inversion on the $2p_1 \rightarrow 1s_4$ transition.

a voltage signal (S) is derived which is proportional to n in Eq. (A1). Thus,

$$S=kn. \tag{A2}$$

The total signal-to-noise ratio in this voltage signal may be determined from the sum of the separate variances in the output voltage originating from each of the random multiplication processes involved.

If the only random variation occurred in n_0, the signal-to-noise ratio on the output would be

$$(S/N)_0=\sqrt{n_0}\equiv kn/\sqrt{(\mathrm{Var})_0} \tag{A3}$$

due to a Poisson distribution with average number n_0. Hence the variance in the output voltage due to random variations in n_0 alone would be

$$(\mathrm{Var})_0=k^2n_0(\eta_e\eta_1\eta_2\cdots\eta_n)^2. \tag{A4}$$

If the only random variation occurred in the photo-detection efficiency η_e the signal-to-noise ratio on the output would be

$$(S/N)_e=\sqrt{(n_0\eta_e)}\equiv kn/\sqrt{(\mathrm{Var})_e} \tag{A5}$$

and therefore the variance of the output due to random variations in the photo-efficiency alone would be

$$(\mathrm{Var})_e=k^2n_0\eta_e(\eta_1\eta_2\cdots\eta_n)^2. \tag{A6}$$

Similarly, the variance of the output due to random variations in the ith electron multiplication stage alone is

$$(\mathrm{Var})_i=k^2n_0\eta_e\eta_1\eta_2\cdots\eta_i(\eta_{i+1}\cdots\eta_n)^2. \tag{A7}$$

The total variance on the output due to all of these random processes is given by the sum of the separate variances:

$$(\mathrm{Var})_{\mathrm{total}}=k^2n_0\eta_e\eta_1\eta_2\cdots\eta_n \times[1+\eta_n+\eta_{n-1}\eta_n\cdots+(\eta_e\eta_1\cdots\eta_n)]. \tag{A8}$$

Consequently, the total signal-to-noise ratio on the output is

$$(S/N)_{\mathrm{total}}=kn/(\mathrm{Var})_{\mathrm{total}}$$

$$=\left(\frac{n_0\eta_e\eta_1\eta_2\cdots\eta_n}{1+\eta_n+\eta_{n-1}\eta_n+\cdots+(\eta_e\eta_1\eta_2\cdots\eta_n)}\right)^{1/2}. \tag{A9}$$

Equation (A9) is the same result obtained by Arcese[13] in a somewhat different manner. In the case where all the electron multiplication factors (η) are constant and $\eta^{n+1}\gg1$, Eq. (A9) becomes

$$(S/N)_{\mathrm{total}}\approx(n_0\eta_e)^{1/2}((\eta-1)/(\eta+\eta_e))^{1/2} \tag{A10}$$

For the tubes used in the present experiment, $\eta\approx4$ and $\eta_e\approx0.2$. Consequently, for these tubes Eq. (A10) predicts signal-to-noise ratios which are smaller than $(n_0\eta_e)^{1/2}$ by about 20%.

In the present experiment an output pulse is derived from the photomultiplier tube from the emission of a photoelectron at the cathode. This pulse is fed through an amplifier, an integral pulse amplitude discriminator and it is then counted by a scaler. The average frequency of occurrence of photoelectron pulses is low enough for the circuitry to count all such events. However, the secondary electrons which give an average current gain $\approx10^6$, arrive at the last dynode within a time interval ≈2 nsec and are not individually resolved. The number of events counted is therefore comparable to $n_0\eta_e$, rather than Eq. (A1). Variations in the total number of secondary electrons reaching the last dynode from random variations in the multiplication process still affect the actual signal-to-noise ratios in the experiment, however, because output pulses that occur with amplitudes below the discriminator threshold are not counted. If no events were missed by the discriminator, the limiting signal-to-noise ratio from Eq. (A9) would approach

$$(S/N)_{\mathrm{photoelectron}}=[n_0\eta_e/(1+\eta_e)]^{1/2}, \tag{A11}$$

where $n_0\eta_e$ is the average number of photoelectrons. Hence the limiting signal-to-noise ratio would be decreased from $(n_0\eta_e)^{1/2}$ by $\approx10\%$ for the present tubes.

The exact fraction of the pulse-height distribution which is missed by the discriminator in the experiment is not known. However, it seems probable that at least $\gtrapprox\frac{1}{2}$ of the total number are missed due to the necessity of setting the discriminator appreciably above the other noise sources in the present wide band system. Hence, the actual signal-to-noise ratio in the system is probably nearer to that predicted by Eq. (A10) than that from Eq. (A11). Consequently, we have increased the weighted standard deviations used in the reduction of data in the present experiment by 20% from the square root of the number of counts measured in each delayed coincidence channel.

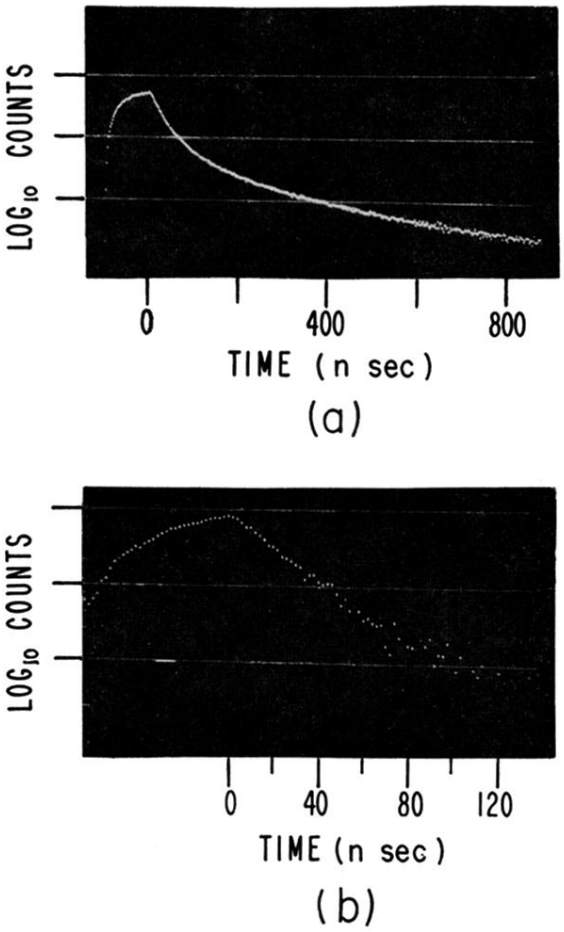

FIG. 5. Data taken on the $2p_2$ lifetime illustrating the effects of radiative cascade. The excitation pulse was turned off at time $t=0$ in each figure. The data in Fig. 5(a) correspond to an electron energy 11 eV above threshold and are characterized by more than 3 exponential decay terms. Fig. 5(b) was taken $\approx$0.1 eV above threshold and contained only one exponential component within the statistical accuracy. (See Fig. 6 and Table I.)

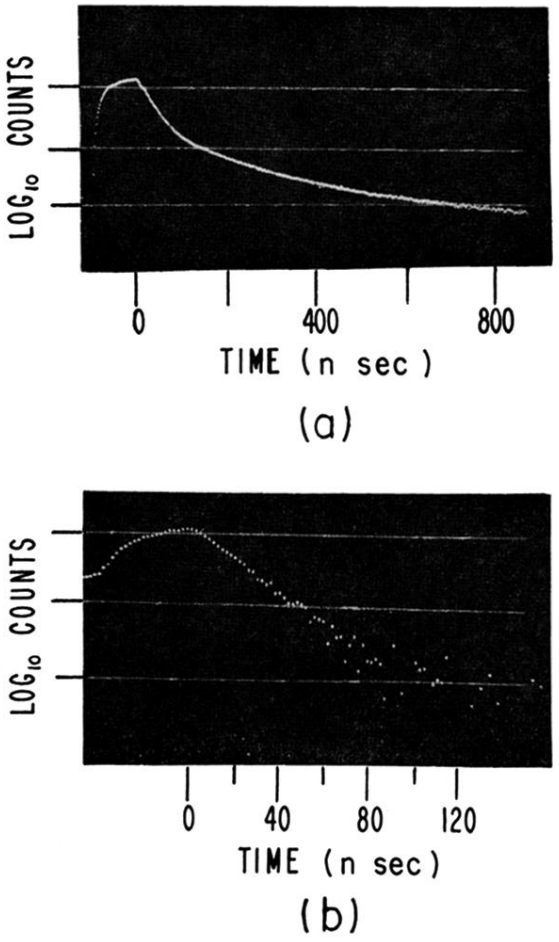

FIG. 6. Data taken on the $2p_8$ lifetime illustrating the effects of radiative cascade. Figure 6(a) corresponds to 11 eV above threshold and Fig. 6(b) corresponds to $\approx$0.1 eV above threshold. (See Fig. 5 and Table I.)